www.czasopisma.pan.pl PAN POLSKA AKADEMIA NAUK www.journals.pan.pl

Arch. Metall. Mater. **67** (2022), 3, 975-985

DOI: https://doi.org/10.24425/amm.2022.139691

M.M. LACHOWICZ[1], M. WINNICKI[1*]

CORROSION DAMAGE MECHANISMS OF TiO_2 COLD-SPRAYED COATINGS

Cold spraying as a low-temperature coating deposition method is intended for thermally sensitive materials. Due to its precise temperature control, it limits the formation of structural defects, and can therefore be easily applied to spray corrosion protective coatings made from metal or metal-ceramic powders. However, the formation of pure ceramic coatings with the use of cold spraying is still not so common. Titanium dioxide is one of the most interesting ceramics due to its photocatalytic properties. Nevertheless, these types of coating materials usually work in a corrosion favoring humid atmosphere. In the presented paper, amorphous TiO_2 powder was deposited onto aluminum alloys and steel substrates and then submitted to potentiodynamic corrosion tests in a 3.5 wt.% NaCl solution. The as-sprayed coating showed phase transition from amorphous TiO_2 to anatase, and also revealed porosity. As a result, electrolytes penetrated the coating and caused undercoating corrosion in the tested environment of an aqueous NaCl solution. The analysis of the potentiodynamic curves showed that the presence of the coating decreased corrosion potential on both substrates. It arose from the mixed phases of TiO_2, which consisted of photocathode – amorphous material and photoanode – crystalline anatase. The phase mixture induced the galvanic corrosion of metallic substrates in the presence of electrolytes. Moreover, pitting-like corrosion and coating delamination were detected in aluminium alloy and steel samples, respectively. Finally, the corrosion mechanism of the titanium dioxide coatings was characterized and described.

Keywords: titanium dioxide; cold-sprayed coatings; potentiodynamic polarization tests; aluminum alloys; structural steel

1. Introduction

Titanium dioxide is a promising semiconductor that is frequently used in many applications, e.g. dye-sensitized solar cells for photovoltaic devices [1,2], self-cleaning and antimicrobial coatings [3], optical filters that protect from ultraviolet rays from the sun [4,5], energy storing as a base for anodes in Li-ion batteries [6], electrochromic displays [7], and also humidity [8] and gas sensors [9]. This metal oxide is widely used as a photocatalyst in water or air purification systems due to its advanced oxidation processes and non-toxic and corrosion resistance properties [10], [11]. Titanium dioxide exhibits three crystalline polymorphs: brookite, anatase and rutile, which are the only thermodynamically stable forms. Nevertheless, anatase is considered as a better photocatalyst than rutile, which is due to the bulk transport of excitons to the surface. In anatase coatings, charge carriers from deeper in the bulk reach the surface and contribute to reactions, while in rutile they recombine before reaching the surface [12]. Therefore, anatase has become an interesting candidate as an n-type photoanode due to its excellent efficiency in generating electron-hole pairs [13].

The preparation of nanostructured ceramic material with a controlled chemical composition, nanoparticle size distribution and uniformity requires chemical methods such as sol-gel [14]. This method enables various materials to be prepared with the highest precision. The combination of sol-gel with one of the liquid deposition techniques, e.g. dip-, spin- or spray- coating, results in the deposition of a thin, uniform and dense coating. Nevertheless, the liquid state of the material requires post-deposition heating, which usually causes shrinkage of the coating and the formation of defects [15]. There are also other TiO_2 coating formation methods, e.g. spray pyrolysis [16], hydrothermal synthesis [17], chemical vapor deposition (CVD) [18], pulsed laser deposition (PLD) [19], atomic layer deposition (ALD) [20], and ion sputtering [21]. However, the methods listed above mainly provide a thin thickness, and thus proper adhesion of the films and their long-term stability are difficult to achieve [22]. Thermal spraying methods enable dense and thick coatings to be created, however, the process temperature limits their application to thermally stable materials [23]. The spraying of anatase powder mainly results in the final coating being transformed to rutile. An interesting option is the cold spray method, which utilizes working gas with a low temperature.

[1] WROCŁAW UNIVERSITY OF SCIENCE AND TECHNOLOGY, DEPARTMENT OF METAL FORMING, WELDING AND METROLOGY, 5 LUKASIEWICZA STR., 50-371 WROCLAW, POLAND

* Corresponding author: marcin.winnicki@pwr.edu.pl

Cold spraying is a solid state process that operates with working gas (usually air, nitrogen or helium), which is accelerated to supersonic velocity by a convergent-divergent de Laval nozzle. Powder particles are introduced to the nozzle in the vicinity of the nozzle's throat and gain velocity from the flowing gas. What is more, preheated gas increases the temperature of the powder particles and simultaneously increases the plasticity of the material prior to impact onto the substrate. Consequently, the coating is formed mostly due to the high kinetic energy of the particles, in turn limiting the influence of thermal energy [24]. It is worth stressing that cold spraying was designed for plastic materials, e.g. metals or polymers. Ceramic powder is only used to increase the density of the coating. This is due to the fact that it has a tamping effect on metal particles [25]. The latest research has shown that pure ceramics can be also sprayed, which in turn form dense and thick coatings [26]. Nevertheless, the selection of an appropriate powder morphology is crucial. The agglomerates of submicron or nanosized ceramic powders are able to absorb impact energy, fracture, and then form dense coatings [27]. However, sintering powders exhibit strong bonds between particles, thus changing their morphology [28]. Therefore, it was proposed to use amorphous TiO_2 powder synthesized by the sol-gel method to form a thick coating by cold spraying without any post-treatment [29]. Furthermore, a phase transition of the amorphous phase into crystalline anatase occurred due to the high kinetic energy of the spraying process. Nevertheless, structure defects, e.g. microcracks or micro-porosity, decreasing mechanical properties, and corrosion resistance were locally found in the coating [27,29].

Titania is known as a corrosion resistant material. Many researchers have tested the application of TiO_2 coatings against various corrosive atmospheres, mainly using the following deposition techniques: the electrochemical anodization process [30-32], magnetron sputtering [3,33], dip- or spray- coating [3,10,34], and plasma or HVOF spraying [35-37]. However, the defects of the coatings usually enabled the penetration of electrolytes and put the substrate at risk of corrosion. The applications of TiO_2 coated materials include moisture-saturated air, such as corrosive marine [38,39] or tropic [40] climate with high atmospheric humidity or underwater conditions [41-43]. As a result the electrochemical corrosion can be enhanced by pollutants, e.g. chlorine [44] or sulfur [45]. Therefore, in this study, amorphous powder was deposited by low-pressure cold spraying to form an anatase coating on various substrates, with the corrosion resistance of the material pair then being assessed. The aim of the research was to determine the mechanism of the corrosion destruction of the coating, which is used for application as a photocatalyst.

2. Experimental tests

2.1. Preparation of materials and coatings

Amorphous TiO_2 powder was used as a feedstock material in the cold spraying process. Detailed sol-gel synthesis of the powder was described in previous work [46]. As-synthesized powders form large agglomerates up to 70 µm and consist of small regular and nearly spherical particles with a diameter of about 600 nm. The general view of amorphous TiO_2 powder is shown in Fig. 1.

The substrate materials were a disk of AA1350 aluminum alloy and structural steel (grade S235JR) with a diameter and thickness of 15 mm and 3 mm, respectively. The surface of the substrates prior to spraying was degreased and sand blasted under a pressure of 0.6 MPa using alumina powder (mesh 45).

The low-pressure cold spraying was performed using the DYMET 413 device (Obninsk Center for Powder Spraying, Obninsk, Russia). A spraying gun with a circular de Laval nozzle with an outlet diameter of 5 mm and radial powder feeding was used in the process. A manipulator (BZT Maschinenbau GmbH, Leopoldshöhe, Germany) moved the gun with a traverse speed of 5 mm/s along parallel lines with 2 mm intervals. The stand-off distance was established to 10 mm. Air with pressure of 0.5 MPa, which was preheated to 600°C, was used as the working gas. An aerosol powder feeder (RBG 100D, Palas, Karlsruhe, Germany)

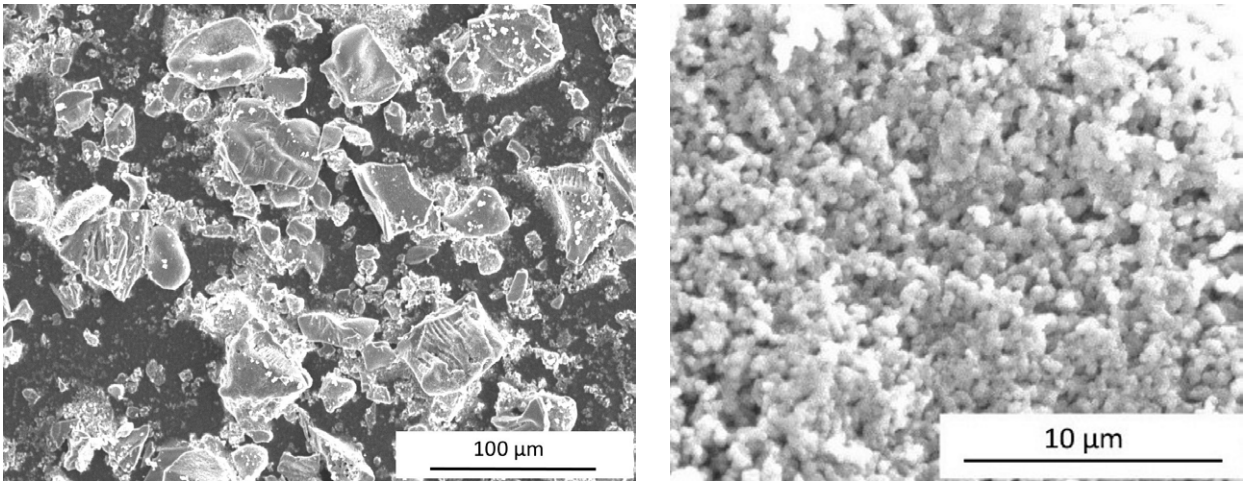

a) b)

Fig. 1. Amorphous TiO_2 powder produced by the sol-gel method: a) agglomerates and b) submicron particles, SEM

TABLE 1

Chemical composition of the investigated materials

Alloy	Chemical composition wt%									
	Al min	Si max	Fe max	Cu max	Mn max	Cr max	Zn max	Other		
								V+Ti max	Ga max	B max
AA 1350 (PN-EN 573-3:2010)	99.5	0.1	0.40	0.05	0.01	0.01	0.05	0.02	0.03	0.05
	Fe	C max	P max	S max	N max					
S235JR PN-EN 10025-1:2007	bal	0.2	0.045	0.045	0.009					

enabled a precise powder feeding of 0.34 g/min. Nitrogen (Nitrogen 4.0, Linde gas) under the pressure of 0.1 MPa worked as the powder transporting gas.

2.2. Characterization of the coatings

Before and after the corrosion tests, the samples underwent surface and cross-section analysis using Scanning Electron Microscopy (SEM) (Phenom X-Pro Scanning Electron Microscope, Thermo Fisher Scientific, Eindhoven, the Netherlands) equipped with SE, BSE detectors and the EDS system for elemental analysis. The specimens for metallographic assessment were prepared by cutting the sample in the middle of its length. The cross-sections were then mounted in epoxy resin, grounded with sand-paper and polished with diamond suspension.

X-ray diffraction analyses were performed on the feedstock powder, as well as on cold sprayed coatings to identify the phases present on their surface. XRD measurements were carried out using the Rigaku Ultima IV Diffractometer with Cu Ka irradiation (k = 1.5406 A°) within the range from 10° to 60° in 0.02° steps with an exposure time of 4 s per point.

The electrochemical properties of the coatings and the uncovered substrates were investigated with the use of an ATLAS 0531 electrochemical unit (ATLAS-SOLLICH, Rębiechowo, Poland) by conducting anodic polarization measurements following the PN EN ISO 17475:2008U standard,. The electrochemical cell included a three-electrode system with an austenitic steel electrode and a silver/silver chloride (Ag/AgCl) electrode, which were used as auxiliary and reference electrodes, respectively. The third electrode was a specimen with a flat surface of 78.5 mm^2. Prior to the measurements, the samples were exposed to open circuit potential stabilization in a solution of 3.5 wt.% NaCl and at a temperature of 20°C. The open corrosion potential (E_{OCP}) of the coated samples was measured to define the range of experimental potentials in the electrochemical experiments. The potential was scanned from 0.2 V below the resulting potential (E_0), and then increased to a potential of 1 V at a scanning rate of 1 mV/s. In order to estimate the values of the corrosion rate (I_{corr}) and corrosion potential (E_{corr}), Tafel experiments were carried out on the cold sprayed coatings. For comparison, curves of the technical aluminum alloy and steel substrate were also measured under the same conditions.

3. Results and discussion

3.1. Microstructural features of the coatings

The deposited TiO_2 coatings had a continuous and uniform surface (Fig. 2a and 3a). Nevertheless, the coating sprayed on the aluminum alloy substrate showed a more developed surface

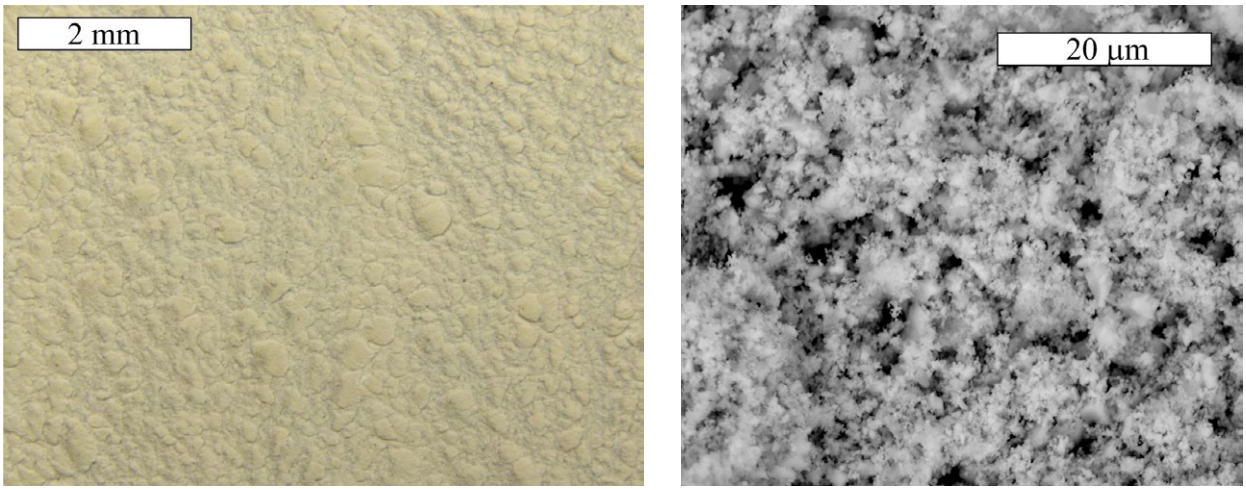

a) b)

Fig. 2. Images of the TiO_2 coating deposited onto the aluminum substrate in macroscale (stereoscopic microscope) (a) and microscale (SEM, BSE) (b)

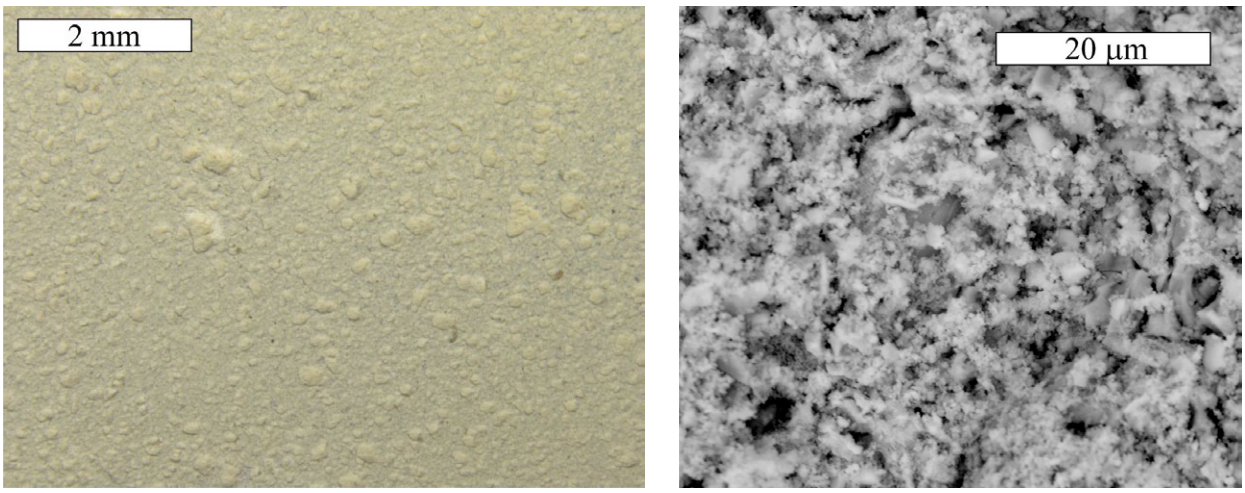

a) b)

Fig. 3. Images of the TiO_2 coating deposited onto the steel substrate in macroscale (stereoscopic microscope) (a) and microscale (SEM, BSE) (b)

topography, in turn resulting in a higher roughness (TABLE 2). AA1350 alloy consists mostly of aluminum (99.6 wt.%), and is thus characterized by small hardness. Therefore, sand-blasting provided an increased roughness when compared to the structural steel. As a result, a higher deposition efficiency and surface development of the coating was achieved. It is worth stressing that the micro-porosity of the surface of the coatings was observed in the SEM images (Fig. 2a and 3b), which was due to the weakly bonded TiO_2 particles in the surface region. There were no incoming particles to densify the coatings. Furthermore, the coatings were deposited with amorphous TiO_2 powder, and according to XRD patterns, anatase was formed in the coatings (Fig. 4). Despite the low process temperature, phase transition into crystalline anatase was still initiated, which resulted from the high kinetic energy of the cold spray process [24,29].

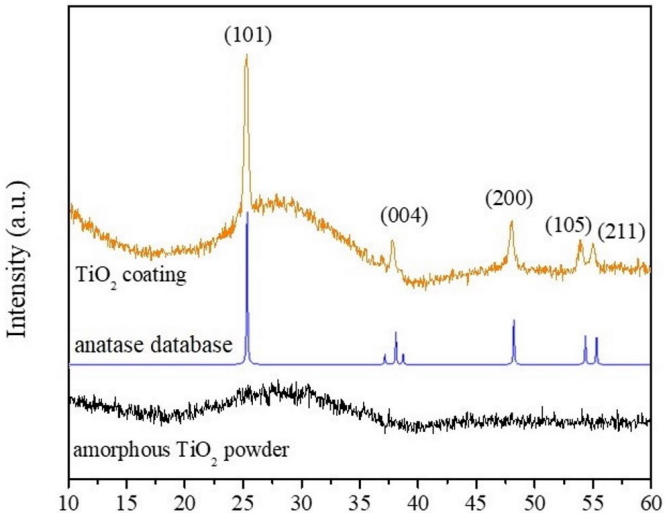

Fig. 4. XRD patterns of the TiO_2 powder after sol-gel synthesis, and the coatings deposited using the LPCS method

TABLE 2

Roughness measurements of the TiO_2 coatings

Material	Ra [µm]
S235JR – SB	4.74
S235JR – AS	6.88
Al – SB	6.45
Al – AS	8.54

where: SB – sand-blasted substrate surface
AS – as-sprayed coating surface

3.2. Electrochemical properties of the coatings

The results of the potentiodynamic corrosion test in 3.5 wt% NaCl solution are presented in Fig. 5 and 6, while electrochemical parameters are collected in TABLE 3. The samples with deposited TiO_2 coatings on both substrate materials showed a shift of corrosion potential of about 150 mV to a more negative direction. The analysis of the potentiodynamic curve showed that the aluminum alloy in the sodium chloride solution did not passivate, but instead started to oxidize. The presence of the coating increased the corrosion current density (I_{corr}) when compared to the substrate, and also decreased its corrosion potential (E_{corr}). The corrosion potential determines the susceptibility of a material to corrode, while the corrosion current density defines its corrosion rate. Nevertheless, the presence of the coating clearly inhibits anodic processes, which can be seen by the fact that the curve is flat in the diagram. In the case of the steel, both the samples (with and without the coating) showed a similar curve shape (see Fig. 6). However, the samples with the deposited coating revealed a lower corrosion potential. Wang et al. [47] sprayed titanium coating onto chromium steel and also obtained a greater electronegative corrosion potential of the sample when compared to non-coated steel. On the other hand, the authors of work [47] increased corrosion resistance by polishing the surface of the coating. Nevertheless, in the case of ceramic coating applied to corrosion protection, the subject is more complicated. In semiconductor photoelectrochemical cathodic protection, the

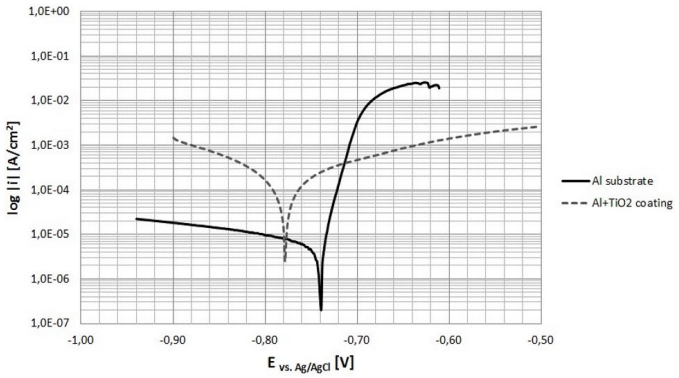

Fig. 5. Polarisation behaviour of the aluminum alloy substrate and the deposited TiO_2 coating

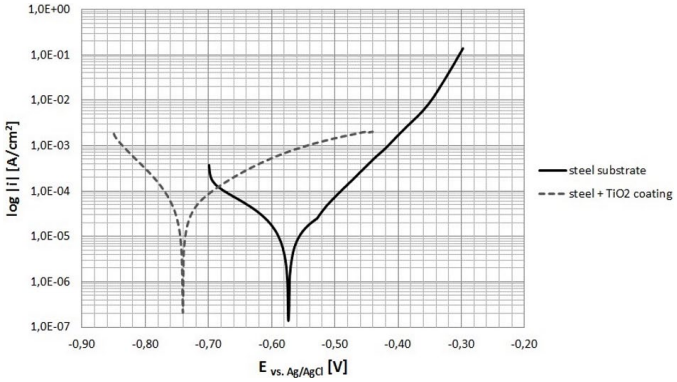

Fig. 6. Polarization behavior of the steel substrate and the deposited TiO_2 coating

conduction band (CB) potential of the semiconductor must be more negative than the self-corrosion potential of the protected metal. As a result, electrons will be provided to the protected metal. The metal can then be oxidized by the oxidizing species, causing the metal corrosion to be replaced. When the electron transfer rate to the metal is properly high, the electrons will polarize the potential of the metal to a more negative region [48]. Kumari et al. [49] showed that the corrosion potential of HA-TiO_2 (1:1 wt%) shifted towards the active direction when compared to Ti6Al4V substrate during tests in Hang's solution. This was due to the porosity and induced galvanic corrosion by partially amorphous HA and TiO_2 particles in the coating. What is more, Kumari et al. [49] observed a decrease in the corrosion rate and an increase in the pitting potential after heat treatment of the coating, which was possibly due to (a) the amorphous to crystalline phase transformation, (b) microstructural homogenization, and (c) the reduction in porosity. TiO_2 in the form of anatase has been known to be an efficient photoanode [50]. Nevertheless, the latest research has shown the potential of amorphous TiO_2 to be a photocathode in photoelectrochemical cells [51]. In this case, coatings deposited from amorphous TiO_2 powder, and which contain a mixture of amorphous powder and crystalline anatase, will induce the galvanic corrosion of metal substrate in the presence of electrolytes. This is the main reason why the corrosion potential shifted towards negative values. Song et al. [52] plasma sprayed Al_2O_3-TiO_2 with low current density (6.3×10^{-8} A/cm^2) in the passive region, low corrosion potential (–0.55 V) and no pitting corrosion, and thus concluded that corrosion resistance can be enhanced by low porosity and smooth surface roughness. What is more, Bakhsheshi-Rad et al. [53] sprayed TiO_2 by high velocity oxygen fuel (HVOF) and obtained E_{corr} of –0.74 V and –0.58 V for the coated to uncoated samples, respectively. The decrease of corrosion potential was related to the porosity and microcracks, which provided penetration locations for the electrolyte to the substrate.

In the tested environment of the aqueous NaCl solution, the coatings showed anodic behavior with regards to both substrate materials. A typical feature of anodic coating is the presence of a large anodic surface. Therefore, TiO_2 coatings with internal porosity should protect aluminum alloy or steel substrate, with both having cathodic behavior. In an anodic-cathodic system, an active material (an anode) corrodes with a higher corrosion rate, while a noble material (a cathode) is protected. In the case of the applied metal coating, in such a system the coating would corrode. Nevertheless, in the performed tests, the coating was made of TiO_2 that was resistant to corrosion, but due to the porosity, an undercoating corrosion occurred. What is more, the presence of porosity and microcracks prevented the generation of a passive layer of the substrate. Bakhsheshi-Rad et al. [53] concluded that the concentration of the dissolved oxygen in the microcracks is low, while the concentration of Cl^- ions dominate, in turn causing the change of the surrounding metal from a passive to active state during potentiodynamic tests of HVOF TiO_2 coating in 3.5 wt.% NaCl solution.

TABLE 3

Electrochemical parameters obtained for the substrates and coatings

	E_{OCP} [V]	E_{corr} [V]	I_{corr} [μA/cm^2]
Steel substrate	–0.54	–0.58	5.63
Steel + coating	–0.66	–0.74	23.4
Aluminum alloy substrate	–0.75	–0.74	2.89
Aluminum alloy + coating	–0.76	–0.78	64.6

3.3. Corrosive features of the coatings

The surface of the coatings after the corrosion tests is presented in Fig. 7-9. A general feature of the coatings deposited onto the aluminum alloy and steel substrates is presented in Fig. 7. As a result of undercoating corrosion, a loss of adhesion, followed by delamination, occurred. Furthermore, the course of the electrochemical processes depended on the substrate material.

The aluminum alloy in the presence of the TiO_2 coating degraded by forming an aluminum oxide layer (see Fig. 8a). In fact, a pitting-like corrosion morphology was detected, mainly at the pre-existing porosities. The porosity of the coatings was responsible for the penetration of the corrosion solution by capillary forces to the interfacial boundary of the substrate and the

coating material. As a result, corrosion microcells were initiated. What is more, microscopic analysis of the corrosive changes showed features of a crystallographic attack (Fig. 8b), which is connected with privileged paths that enable propagation of corrosion along the {100} plane and crystallographic direction of <100> [54-58].

The corrosion tests of the TiO_2 coatings deposited on the steel substrate showed similar results. The corrosion behavior was nonuniform (see Fig. 9). An electrolyte penetrated the coating due to the presence of material discontinuities, in turn causing oxidation of the steel. The increasing volume of corrosion products generates tensile stresses at the interfacial boundary between the substrate and the coating, finally resulting in coating delamination. As a result, the solubilization of the steel substrate proceeded and revealed a material structure with ferrite and pearlite grains boundaries. A detailed analysis confirmed that the corrosion was initiated in the ferrite region (see Fig. 10b), which arose from the cathodic behavior of the pearlite's cementite.

The corrosion products formed in a ring shape on the steel surface, which suggests that local corrosion was initiated by a cell of heterogeneous aeration (see Fig. 9b). This specific cell forms when Fe^{2+} ions migrating from regions with a lower oxygen concentration meet hydroxide ions migrating from the cathodic region. Furthermore, local filiform corrosion was also noticed, confirming the presence of oxygen cells (Fig. 10a).

Figs 11 to 13 show the cross-sectional morphologies of the coatings after electrochemical examination. Aluminum alloy corrosion was initiated as a result of the penetration of the corrosive solution and oxygen through porous material under the action of capillary forces. Moreover, the corrosion products that are formed on the aluminum surface, as a result of ion diffusion, moved in the area of the fracture, which led to its mechanical

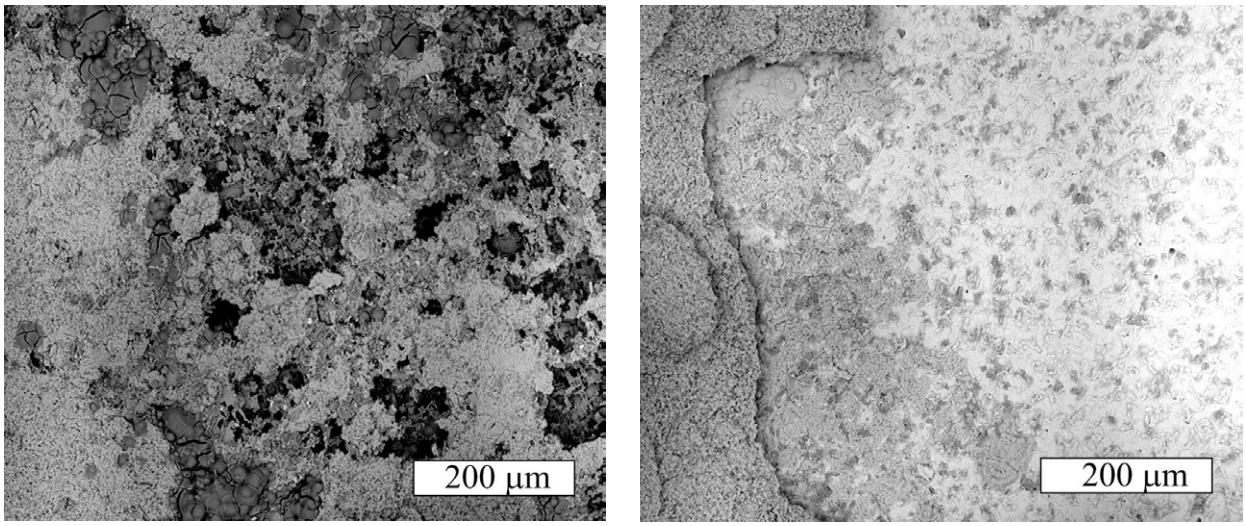

a) b)

Fig. 7. SEM micrographs of corrosion changes (SEM) on the surface of the TiO_2 coating deposited onto the aluminum alloy (a) and steel (b) substrate after the potentiodynamic tests

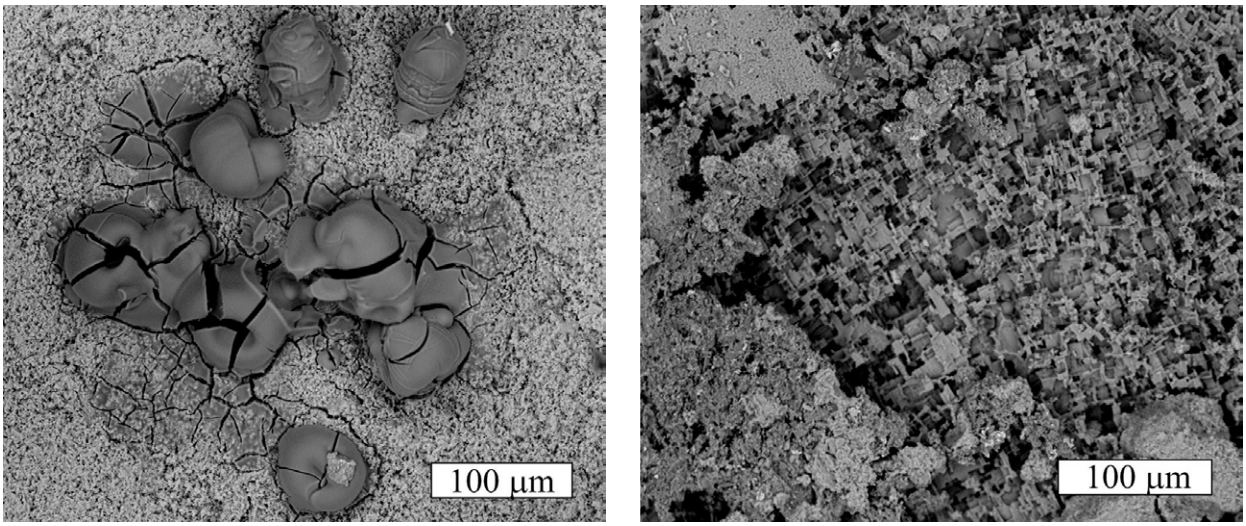

a) b)

Fig. 8. SEM micrographs of corrosion products of the aluminum alloy (a) and crystallographic attack of the substrate (b) noticed by SEM on the surface of the TiO_2 coating

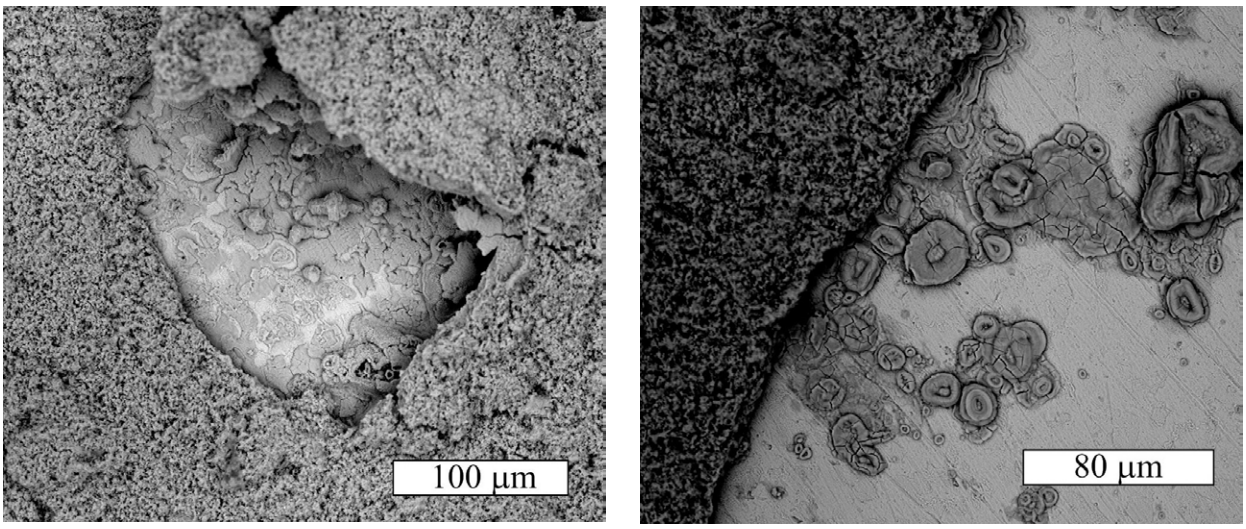

a) b)

Fig. 9. SEM micrographs of corrosion changes (a) and ring-shaped corrosion products (b) at the surface of the steel substrate uncovered by the detached coating

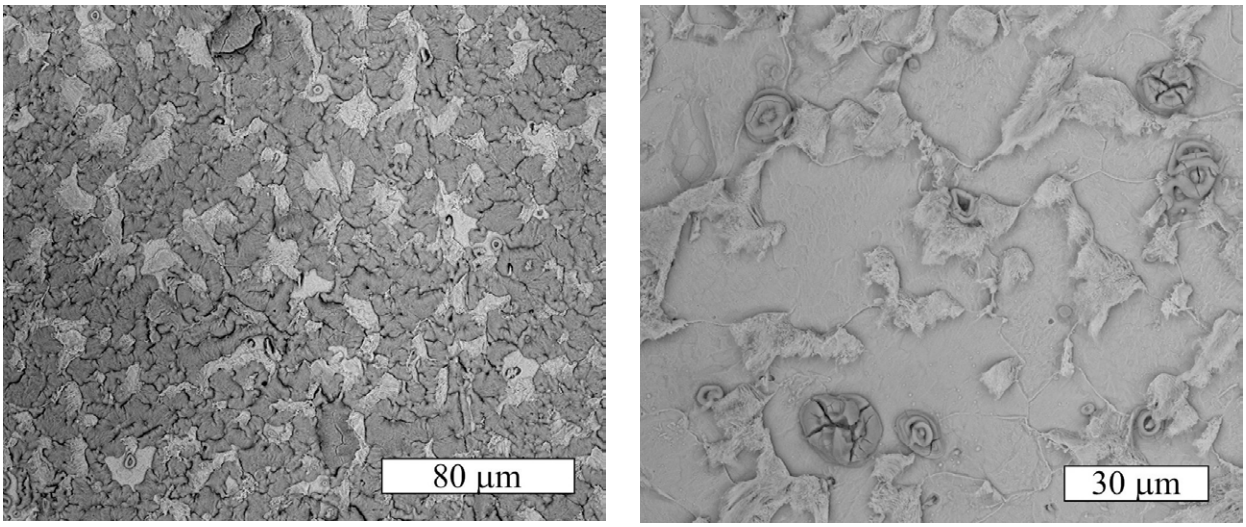

a) b)

Fig. 10. SEM micrographs of corrosion changes on the surface of the steel substrate after detachment of the TiO_2 coating. Presence of filiform corrosion (a) and corrosion initiation in the region of ferrite (b)

widening (the so-called wedge effect). This allows for further penetration of the corrosive solution. Therefore, EDS analysis indicated the presence of aluminum inside the coating.

In the case of the steel samples, the corrosion was penetrating the substrate material (Fig. 13). Substrate preparation prior to spraying with the use of abrasive blasting [59] and the Cold Spray process (as a result of hard particle impacts) [60] causes the cold-work hardening of the substrate in its near-surface area. As a result, the material was weakened and locally active places that initiated corrosion were generated [61]. Furthermore, the formation of corrosion products lifted some parts of the substrate material, which was also visible at the surface of the sample (See Fig. 9a).

A typical route to increase the resistance to corrosion of metal cold sprayed coatings is to decrease the porosity and to increase the thickness of the coating [62]. This can be done by increasing the process parameters in order to achieve a higher strain rate [63], or by mixing ceramic and metal powders to produce a composite coating [60]. Ceramics will act as a hammer, in turn providing a tamping effect and increasing the hardening of metal particles [25,62]. As a result, porosity will be decreased. Other approaches are based on post-spraying heat-treatment of the coating. The annealing will cause recrystallization and grain growth, resulting in the minimizing of porosity [64,65]. However, the first solution, which involves the spraying of just the ceramic, will not work. This is due to the fact that the mechanism of forming the coating of ceramic and metallic particles is different. In turn, the second solution, which includes the sintering of the ceramic particles, should be successful. Yabuki et al. [66] proposed application of TiO_2 particle – polymer composite coat-

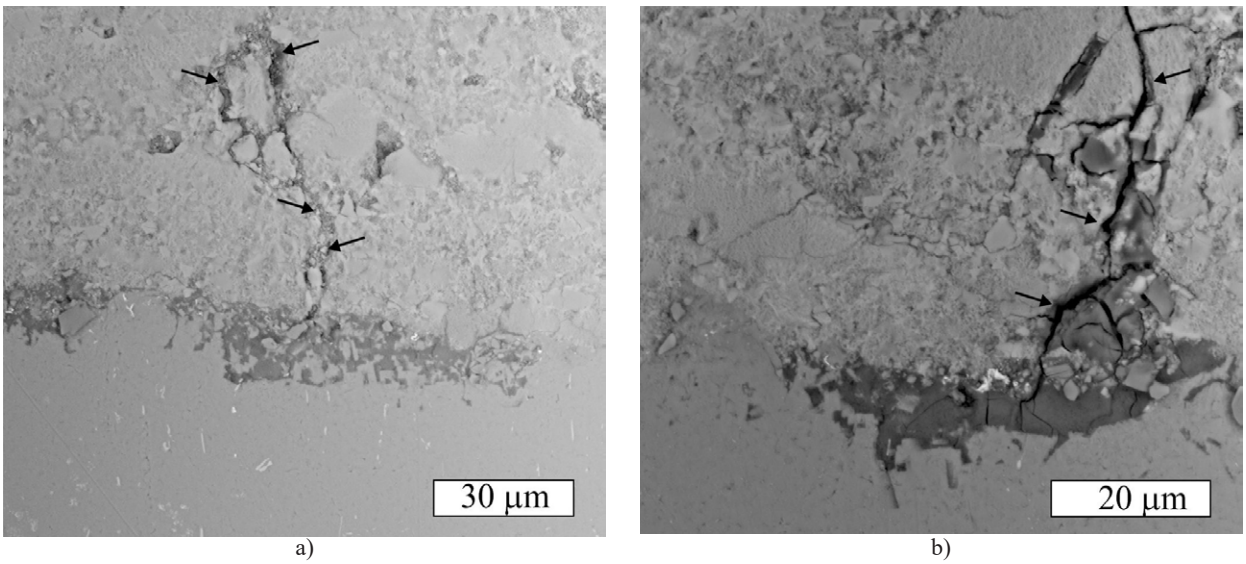

a) b)

Fig. 11. SEM cross-section images of the TiO_2 coating deposited onto the aluminum alloy substrate after the potentiodynamic tests

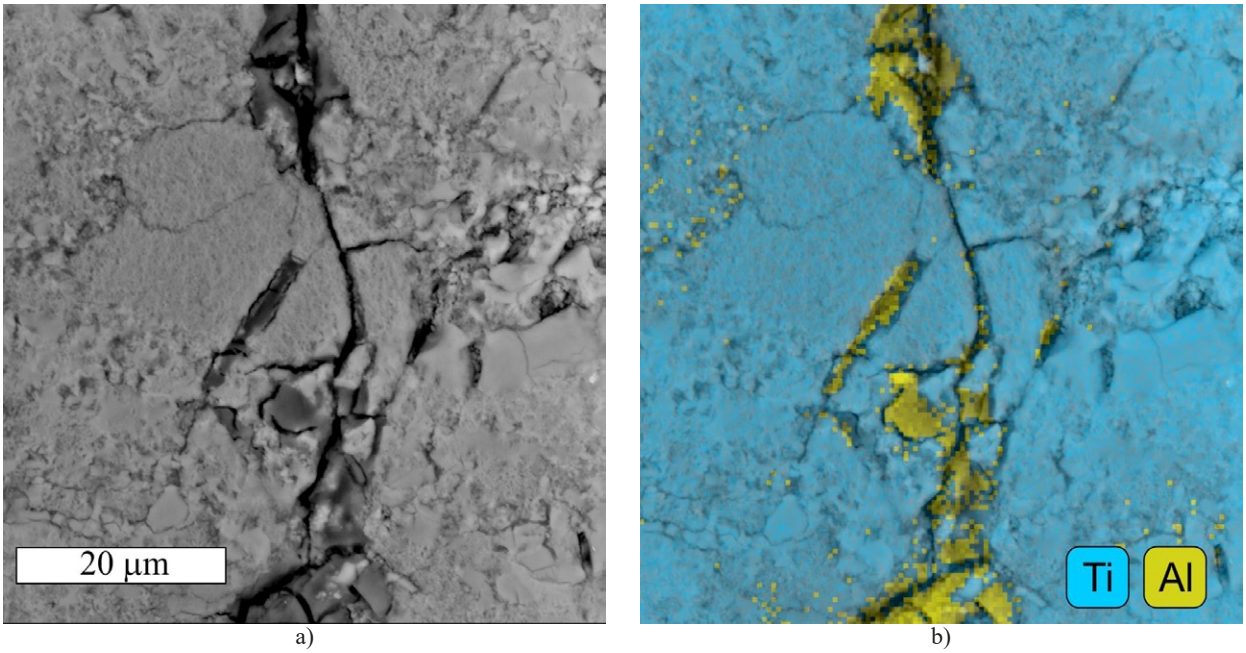

a) b)

Fig. 12. SEM cross-section image (a) and EDS analysis (b) of the TiO_2 coating deposited onto the aluminum alloy with visible penetration of corrosion products

ings to protect surface of 5083 aluminum alloy. Authors noticed that coating showed self-healing properties as the polarization resistance of the samples increased significantly over time. The corrosion resistance was related to dissolution of polymer – bisphenol A in the presence of TiO_2 particles, which formed a thin film on the surface of aluminum alloy substrate. Naghibi et al. [67] applied design of experiment to analyze the dip-coating process parameters and increased anticorrosion performance of 316L stainless steel by depositing optimized TiO_2 films. Significant increase of corrosion resistance due to TiO_2 Nanoparticle/Trimethoxy(propyl)silane ceramic composite coating deposited by electrophoretic deposition method on 316L stainless steel was also observed by Emarati et al. [68]. It was achieved by the water-repellent protective composite coatings, which prevent the penetration of corrosive agent to the metal substrate.

It is worth emphasizing that the obtained anatase (due to spraying) is sensitive to elevated temperatures. The heat treatment process performed at a temperature of 600°C could initiate phase transition into rutile, which is photovoltaically less active [69]. It should be emphasized that TiO_2 coatings deposited by LPCS are intended for photocatalysis, and thus the obtaining of anatase was crucial. Nevertheless, the structure and properties of coating or substrate material can changed due to working conditions [70,71]. Therefore, new research is needed to find an appropriate process of sintering ceramic particles with the use of light-waves instead of a heat source.

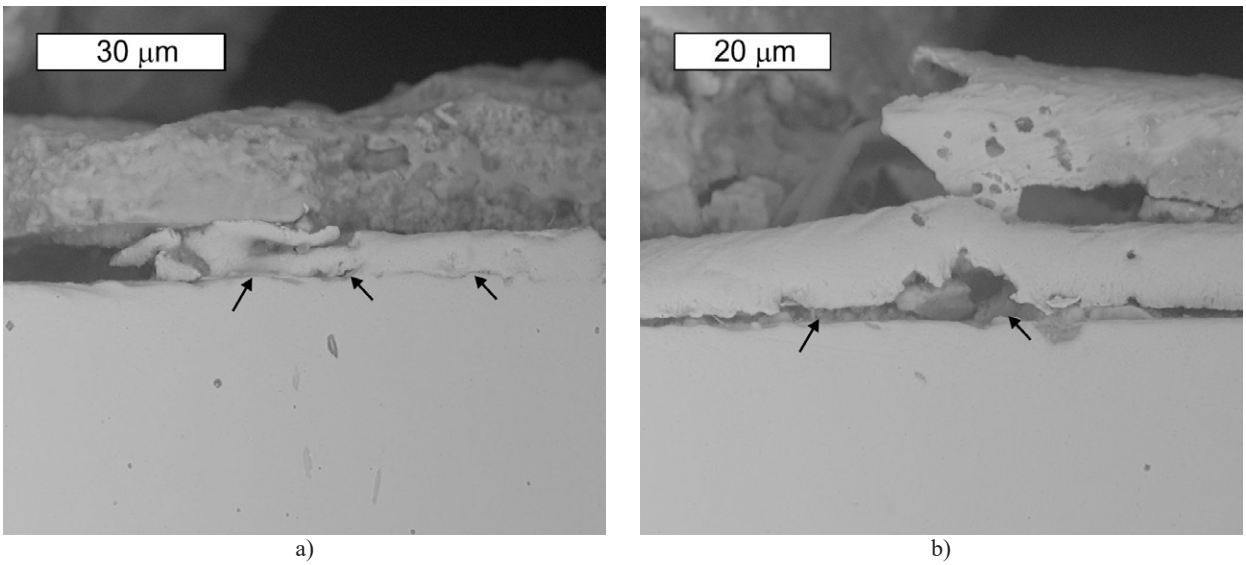

a) b)

Fig. 13. SEM cross-section images of the TiO_2 coating deposited onto the steel substrate after the potentiodynamic tests. Arrows point to the detachment of the substrate's outer region due to corrosion in the cold worked region

4. Summary

In the presented study, TiO_2 amorphous sol-gel powder was deposited by low-pressure cold spraying onto aluminum alloy and steel substrates. The coatings showed a non-uniform structure that had submicron TiO_2 particles mixed with regular crystals of formed anatase. Moreover, porosity was noticed in the surface and inside the coating.

Cold spraying is intended for the deposition of metallic coatings that are applied in corrosive environments. Nevertheless, the presence of porosity in the regions of unbonded fine ceramic particles favor electrolyte penetration. The performed potentiodynamic tests confirmed the anodic behavior of the TiO_2 coatings with regards to both substrate materials in the tested environment of an aqueous NaCl solution. The corrosion potential decreased from –0.58 V to –0.74 V, while corrosion current density increased from 5.63 μA/cm^2 to 23.4 μA/cm^2 for uncoated and coated steel samples, respectively. In the case of aluminum alloy the corrosion potential was similar for both samples, however corrosion current density increased significantly from 2.89 μA/cm^2 to 64.6 μA/cm^2 for uncoated and coated samples, respectively. The corrosion solution penetrated the coating to the interfacial boundary between the coating and the substrate through coating crevices by the action of capillary forces. As a result, a corrosion cell was initiated in the substrate surface, in turn causing undercoating corrosion. The final course of the electrochemical processes depended on the material of the substrate. However, further work is needed to find an appropriate method of compressing ceramic coatings in low temperatures in order to avoid the phase transition of anatase. As discussed earlier, maintaining this phase is crucial with regards to photocatalytic properties.

Acknowledgment

This research was funded by Polish National Science Centre under the Contract No. 2016/23/D/ST8/00675 (Project title: The mechanism of joining submicron ceramic particles in cold spraying process).

REFERENCES

[1] Y.-M. Sung, H.-J. Kim, Thin Solid Films **515**, 4996-4999 (2007). DOI: https://doi.org/10.1016/j.tsf.2006.10.079

[2] K.M.P. Bandaranayake, M.K. Indika Senevirathna, P.M.G.M. Prasad Weligamuwa, K. Tennakone, Coordin. Chem. Rev. **248**, 1277-1281 (2004). DOI: https://doi.org/10.1016/j.ccr.2004.03.024

[3] P. Navabpour, S. Ostovarpour, C. Tattershall, K. Cooke, P. Kelly, J. Verran, K. Whitehead, C. Hill, M. Raulio, O. Priha, Coatings. **4**, 433-449 (2014). DOI: https://doi.org/10.3390/coatings4030433

[4] H.S. Song, Y.J. Yoo, G.J. Lee, K.S. Chang, Y.M. Song, J. Nanomater. **2017**, e2738015 (2017). DOI: https://doi.org/10.1155/2017/2738015

[5] D.S. Hinczewski, M. Hinczewski, F.Z. Tepehan, G.G. Tepehan, Sol. Energ. Mat. Sol. C. **87**, 181-196 (2005). DOI: https://doi.org/10.1016/j.solmat.2004.07.022

[6] Y. Liu, Y. Yang, J. Nanomater. **2016**, e8123652 (2016). DOI: https://doi.org/10.1155/2016/8123652

[7] N. Akkurt, S. Pat, R. Mohammadigharehbagh, M. Özgür, U. Demirkol, A. Olkun, Ş. Korkmaz, J. Mater. Sci: Mater. Electron. **31**, 9568-9578 (2020). DOI: https://doi.org/10.1007/s10854-020-03499-0

[8] W.-P. Tai, J.-H. Oh, Sensor. Actuat. B: Chem. **85**, 154-157 (2002). DOI: https://doi.org/10.1016/S0925-4005(02)00074-6

[9] B. Karunagaran, P. Uthirakumar, S.J. Chung, S. Velumani, E.-K. Suh, Mater. Charact. **58**, 680-684 (2007). DOI: https://doi.org/10.1016/j.matchar.2006.11.007

[10] A. Shanaghi, A.R. Sabour, T. Shahrabi, M. Aliofkhazraee, Prot. Met. Phys. Chem. Surf. **45**, 305-311 (2009). DOI: https://doi.org/10.1134/S2070205109030071

[11] S. Malato, P. Fernández-Ibáñez, M.I. Maldonado, J. Blanco, W. Gernjak, Catal. Today. **147**, 1-59 (2009). DOI: https://doi.org/10.1016/j.cattod.2009.06.018

[12] T. Luttrell, S. Halpegamage, J. Tao, A. Kramer, E. Sutter, M. Batzill, Sci. Rep. **4**, 4043 (2014). DOI: https://doi.org/10.1038/srep04043

[13] K. Hashimoto, H. Irie, A. Fujishima, Jpn. J. Appl. Phys. **44**, 8269 (2005). DOI: https://doi.org/10.1143/JJAP.44.8269

[14] L. Huang, J. Xu, X. Sun, C. Li, R. Xu, Y. Du, J. Ni, H. Cai, J. Li, Z. Hu, J. Zhang, J. Alloy. Compd. **735**, 224-233 (2018). DOI: https://doi.org/10.1016/j.jallcom.2017.11.027

[15] N. Vodišek, A. Šuligoj, D. Korte, U. Lavrenčič Štangar, Materials **11**, 1945 (2018). DOI: https://doi.org/10.3390/ma11101945

[16] Y. Doubi, B. Hartiti, L. Hicham, S. Fadili, A. Batan, M. Tahri, A. Belfhaili, P. Thevnin, Mater. Today: Proc. **30**, 823-827, (2020). DOI: https://doi.org/10.1016/j.matpr.2020.04.186

[17] Z.G. Wu, Z.M. Ren, L. Li, L. Lv, Z. Chen, Sep. Purif. Technol. **251**, 117328 (2020). DOI: https://doi.org/10.1016/j.seppur.2020.117328

[18] H. Nagasawa, J. Xu, M. Kanezashi, T. Tsuru, Mater. Lett. **228**, 479-481 (2018). DOI: https://doi.org/10.1016/j.matlet.2018.06.053

[19] F.S. Al mashary, J.F. Felix, S.O. Ferreira, D. de Souza, Y.G. Gobato, J. Chauhan, N. Alexeeva, M. Henini, A.M. Albadri, A.Y. Alyamani, Mater. Sci. Eng: B. **259**, 114578 (2020). DOI: https://doi.org/10.1016/j.mseb.2020.114578

[20] I. Jelovica Badovinac, R. Peter, A. Omerzu, K. Salamon, I. Šarić, A. Samaržija, M. Perčić, I. Kavre Piltaver, G. Ambrožić, M. Petravić, Thin Solid Films **709**, 138215 (2020). DOI: https://doi.org/10.1016/j.tsf.2020.138215

[21] A.M. AL-Baradi, Results Phys. **17**, 103109 (2020). DOI: doi.org/10.1016/j.rinp.2020.103109

[22] N. Vodišek, A. Šuligoj, D. Korte, U. Lavrenčič Štangar, Materials **11**, 1945 (2018). DOI: https://doi.org/10.3390/ma11101945

[23] M. Gardon, J.M. Guilemany, J. Therm. Spray Techn. **23**, 577–595 (2014). DOI: https://doi.org/10.1007/s11666-014-0066-5

[24] T. Schmidt, H. Assadi, F. Gärtner, H. Richter, T. Stoltenhoff, H. Kreye, T. Klassen, J. Therm. Spray Techn. **18**, 794 (2009). DOI: https://doi.org/10.1007/s11666-009-9357-7

[25] H. Koivuluoto, A. Coleman, K. Murray, M. Kearns, P. Vuoristo, J. Therm. Spray Techn. **21**, 1065-1075 (2012). DOI: https://doi.org/10.1007/s11666-012-9790-x

[26] A.R. Toibah, M. Sato, M. Yamada, M. Fukumoto, Mater. Manuf. Process. **31**, 1527-1534 (2016). DOI: https://doi.org/10.1080/10426914.2015.1090587

[27] M. Winnicki, A. Baszczuk, M. Jasiorski, B. Borak, A. Małachowska, Surf. Coat. Technol. **371**, 194-202 (2019). DOI: https://doi.org/10.1016/j.surfcoat.2018.09.057

[28] T.A. Rahim, K. Takahashi, M. Yamada, M. Fukumoto, Mater. Trans. **57**, 1345-1350 (2016). DOI: https://doi.org/10.2320/matertrans.T-M2016817

[29] A. Baszczuk, M. Jasiorski, M. Winnicki, J. Therm. Spray Techn. **27**, 1551-1562 (2018). DOI: https://doi.org/10.1007/s11666-018-0769-0

[30] R. Hazan, S. Sreekantan, R.B.S.M.N. Mydin, AIP Conference Proceedings **2068**, 020013 (2019). DOI: https://doi.org/10.1063/1.5089312

[31] C. Liu, Y. Wang, M. Wang, W. Huang, P.K. Chu, Surf. Coat. Technol. **206**, 63-67 (2011). DOI: https://doi.org/10.1016/j.surfcoat.2011.06.038

[32] M.V. Diamanti, F. Bolzoni, M. Ormellese, E.A. Pérez-Rosales, M.P. Pedeferri, Sci. Technol. **45**, 428-434 (2010). DOI: https://doi.org/10.1179/147842208X373191

[33] J. Liu, Y. Lou, C. Zhang, S. Yin, H. Li, D. Sun, X. Sun, RSC Adv. **7**, 43938-43949 (2017). DOI: https://doi.org/10.1039/C7RA06960J

[34] M. Morozova, P. Kluson, J. Krysa, M. Vesely, P. Dzik, O. Solcova, Procedia Engineer. **42**, 573-580 (2012). DOI: https://doi.org/10.1016/j.proeng.2012.07.450

[35] Y.-S. Song, I.-G. Lee, S.N. Hong, B.-Y. Kim, K.H. Lee, D.Y. Lee, J. Mater. Sci. **41**, 2059-2065 (2006). DOI: https://doi.org/10.1007/s10853-006-4506-6

[36] T.P.S. Sarao, H.S. Sidhu, H. Singh, Metall. Mater. Trans A. **43**, 4365-4376 (2012). DOI: https://doi.org/10.1007/s11661-012-1175-8

[37] F.-L. Toma, C.C. Stahr, L.-M. Berger, S. Saaro, M. Herrmann, D. Deska, G. Michael, J. Therm. Spray Techn. **19**, 137-147 (2010). DOI: https://doi.org/10.1007/s11666-009-9422-2

[38] O. Sengul, M. Kam, Int. J. Anal. Exp. Finite Elem. Anal. **7**, 91-100 (2020). DOI: https://doi.org/10.26706/ijaefea.4.7.20200807

[39] A. Świerczyńska, J. Łabanowski, J. Michalska, D. Fydrych, Mater. Corros. **68** (10), 1037-1045 (2017). DOI: https://doi.org/10.1002/maco.201709418

[40] T. Zhang, X. Xu, Y. Li, X. Lv, Constr. Build. Mater. **277**, 122298, (2021). DOI: https://doi.org/10.1016/j.conbuildmat.2021.122298

[41] S. Kato, K. Hattori, Y. Tanaka, Y. Miyazaki, G. Ishii, S. Koura, N. Negishi, Ceram. Int. **46** (11), 19285-19292 (2020). DOI: https://doi.org/10.1016/j.ceramint.2020.04.268

[42] O.I. Kalu, B. Subramanian, B.J. MacLean, G.C. Saha, Materialia **5**, 100237 (2019). DOI: https://doi.org/10.1016/j.mtla.2019.100237

[43] S. Chang, X. Yang, Y. Sang, H. Liu, Chem-Asian J. **11** (17), 2352-2371 (2016). DOI: https://doi.org/10.1002/asia.201600363

[44] R. Yamanoglu, E. Fazakas, F. Ahnia, D. Alontseva, F. Khoshnaw, Adv. Mater. Sci. **21**, 5-15 (2021). DOI: https://doi.org/10.2478/adms-2021-0007

[45] H.M.A. El-Lateef, M.M. Khalaf, J. Mol. Liq. **331**, 115797 (2021). DOI: https://doi.org/10.1016/j.molliq.2021.115797

[46] A. Baszczuk, M. Jasiorski, B. Borak, J. Wódka, Mater. Sci.-Poland. **34**, 691-702 (2016). DOI: https://doi.org/10.1515/msp-2016-0094

[47] H. Wang, B. Hou, J. Wang, Q. Wang, W. Li, J. Therm. Spray Techn. **17**, 736-741 (2008). DOI: https://doi.org/10.1007/s11666-008-9256-3

[48] Y. Bu, J.-P. Ao, Green Energy & Envir. **2**, 331-362 (2017). DOI: https://doi.org/10.1016/j.gee.2017.02.003

[49] R. Kumari, J.D. Majumdar, Appl. Surf. Sci. **420**, 935-943 (2017). DOI: https://doi.org/10.1016/j.apsusc.2017.05.208

[50] N. Jamalullail, I.S. Mohamad, M.N. Norizan, N. Mahmed, Sol. St. Phen. **273**, 146-153 (2018). DOI: https://doi.org/10.4028/www.scientific.net/ssp.273.146

[51] C.C. Mercado, M.E.L. Lubrin, H.A.J. Hernandez, R.A. Carubio, Int. J. Photoenergy **2019**, 848740, (2019). DOI: https://doi.org/10.1155/2019/9848740

[52] Y.-S. Song, I.-G. Lee, S.N. Hong, B.-Y. Kim, K.H. Lee, D.Y. Lee, J. Mater. Sci. **41**, 2059-2065 (2006). DOI: https://doi.org/10.1007/s10853-006-4506-6

[53] H.R. Bakhsheshi-Rad, M. Daroonparvar, M.A.M. Yajid, P. Kumar, M. Razzaghi, A.F. Ismail, S. Sharif, F. Berto, J. Mater, Eng. Perform. **30**, 1356-1370, (2021). DOI: https://doi.org/10.1007/s11665-020-05333-4

[54] G.M. Treacy, C.B. Breslin, Electrochim. Acta **43** (12-13), 1715-1720 (1998). DOI: https://doi.org/10.1016/S0013-4686(97)00305-8

[55] J.H. Seo, J.H. Ryu, D.N. Lee, J. Electrochem. Soc. **150** (9), B433-B438 (2003). DOI: https://doi.org/10.1149/1.1596952

[56] E.V. Koroleva, G.E. Thompson, P. Skeldon, B. Noble, P. Roy, Soc. **463**, 1729-1748 (2007). DOI: https://doi.org/10.1098/rspa.2007.1846

[57] U. Donatus, G.E. Thompson, J.A. Omotoyinbo, K.K. Alaneme, S. Aribo, O.G. Agbabiaka, T. Nonferr, Metal. Soc. **27** (1), 55-62 (2017). DOI: https://doi.org/10.1016/S1003-6326(17)60006-2

[58] X. Zhang, X. Zhou, T. Hashimoto, B. Liu, Mater. Charact. (130), 230-236 (2017). DOI: https://doi.org/10.1016/j.matchar.2017.06.022

[59] H. Begg, M. Riley, H. de Villiers Lovelock, J. Therm. Spray Techn. **25**, 12-20 (2016). DOI: https://doi.org/10.1007/s11666-015-0324-1

[60] A. Sabard, P. McNutt, H. Begg, T. Hussain, Surf. Coat. Technol. **385**, 125367 (2020). DOI: https://doi.org/10.1016/j.surfcoat.2020.125367

[61] M. Rutkowska-Gorczyca, M. Podrez-Radziszewska, J. Kajtoch, Metall. Foundry Engineer. **35**, 35-43 (2009). DOI: https://doi.org/10.7494/mafe.2009.35.1.35

[62] A. Srikanth, V. Bolleddu, Aust. J. Mech. Engineer. **2020**, 1-22 (2020). DOI: https://doi.org/10.1080/14484846.2020.1794504

[63] K. Balani, T. Laha, A. Agarwal, J. Karthikeyan, N. Munroe, Surf. Coat. Technol. **195**, 272-279 (2005). DOI: https://doi.org/10.1016/j.surfcoat.2004.06.028

[64] R. Huang, M. Sone, W. Ma, H. Fukanuma, Surf. Coat. Technol. **261**, 278-288 (2015). DOI: https://doi.org/10.1016/j.surfcoat.2014.11.017

[65] M.M. Sharma, T.J. Eden, B.T. Golesich, J. Therm. Spray Techn. **24**, 410-422 (2015). DOI: https://doi.org/10.1007/s11666-014-0175-1

[66] A. Yabuki, W. Urushihara, J. Kinugasa, K. Sugano, Mater. Corros. **62** (10), 907-912 (2011). DOI: doi.org/10.1002/maco.201005756

[67] S. Naghibi, A. Jamshidi, O. Torabi, R.E. Kahrizsangi, Int. J. Appl. Ceram. Tec. **11** (5), 901-910 (2013). DOI: https://doi.org/10.1111/ijac.12077

[68] S.M. Emarati, M. Mozammel, Ceram. Int. **46** (2), 1652-1661 (2020). DOI: https://doi.org/10.1016/j.ceramint.2019.09.137

[69] T. Luttrell, S. Halpegamage, J. Tao, A. Kramer, E. Sutter, M. Batzill, Sci. Rep. **4**, 4043 (2014). DOI: https://doi.org/10.1038/srep04043

[70] M. Kam, M. Demirtas, Surf. Rev. Lett. **28** (6), 2150041 (2021). DOI: https://doi.org/10.1142/S0218625X21500414

[71] N. Kubot, M. Ayabet, T. Fukuda, M. Akashi, MRS Online Proc. Lib. **458**, 449-452 (1996). DOI: https://doi.org/10.1557/PROC-458-449